44th AIAA Aerospace Sciences Meeting and Exhibit
9 - 12 January 2006, Reno, Nevada

AIAA 2006-447

Sailplane Performance Improvement Using a Flexible Composite Surface Deturbulator

Sumon.K.Sinha*
Sinhatech
3607 Lyles Drive, Oxford, MS.

Sundeep Vijay Ravande †
Mechanical Engineering Dept.
University of Mississippi

A 5 to 20% increase in the glide ratio of a Standard Cirrus sailplane was observed across its flyable airspeed range by treating 60-100% of the span of the wing upper surface with a Flexible Composite Surface Deturbulator (FCSD) tape. The compliant surface layer of an appropriately positioned narrow FCSD strip undergoes sub-micron scale constrained mode flow-induced oscillations. This encourages the formation of a stable thin and long separation bubble like flow structure in non-zero pressure gradient boundary layers by delaying the breakdown of the shear layer separating the aforementioned bubble from the inviscid external flow. As a result, wind-tunnel tests showed the external flow is accelerated increasing lift, while skin friction is mitigated. This was confirmed by a reduction of the sailplane's induced and parasitic drag components with extended span FCSD treatment. Furthermore, a parallel flight with a higher performance ASW-28 sailplane yielded results that corroborate these measurements.

Nomenclature

A	=	wing planform area
A_r	=	wing aspect ratio
AFW	=	active flexible wall transducer
C_d	=	drag coefficient (D / (qA) for wing), lower case c_d represents the section drag coefficient
C_{di}	=	induced drag coefficient = $C_L^2/(e\pi A_r)$
C_{do}	=	profile or parasitic drag coefficient
C_p	=	pressure coefficient (($p_{static} - p_{static,\infty}$) / q)
Cf	=	Skin Friction Coefficient (τ_w/(qA))
C_L	=	lift coefficient (L / (qA)), lower case c_L represents the section lift coefficient
c	=	airfoil chord length
D	=	drag force
e	=	Oswald span efficiency
s	=	center to center distance between two strips
f	=	FCSD control frequency (U/s)
FCSD	=	flexible composite surface deturbulator
h	=	flight altitude
H	=	kinematic shape factor = δ_1/δ_2
L	=	lift force
M, Ma	=	Mach number
P	=	local static pressure
$p_{static,\infty}$	=	upstream static pressure

* *President,* Sinhatech, Oxford, MS, Senior Member AIAA and Associate Professor of Mechanical Engineering, University of Mississippi

† *Student Member,* AIAA and Graduate Student, University of Mississippi.

$p_{stag,\infty}$ = upstream stagnation pressure
q = up stream dynamic pressure ($\rho\, U^2_\infty /2$), ρ = upstream density
Re = Reynolds number based on the chord length of the airfoil ($\rho\, U_\infty\, c / \mu$)
α = angle of attack
L/D = lift to drag ratio or glide ratio
δ_1 = displacement thickness
δ_2 = momentum thickness
U = local free stream velocity outside boundary layer
U_∞ = upstream velocity
u = fluid velocity in the stream wise direction
v = fluid velocity normal to the stream wise direction
x = distance from the leading edge along chord or streamwise coordinate for flow equations
y = wall normal coordinate for flow equations
τ_w = wall shear stress

I. Introduction

High performance sailplanes represent the pinnacle of aerodynamic efficiency and incorporate the latest drag reduction and construction techniques. Low-roughness all-composite construction, laminar-flow airfoils and winglets have been extensively used on sailplanes before being adopted by other segments of aviation. This is because sailplanes do not rely on engines for propulsion. After being towed to a minimum operating altitude they rely on converting their gravitational potential energy to build up forward speed to generate lift as they glide down. Drag wastes energy, requiring a steeper glide to maintain the requisite forward speed. Altitude is regained when possible by circling in isolated upward hot air drafts or thermals. The challenge for a sailplane pilot is to locate and utilize thermals along the way while maintaining adequate altitude to make it safely to a landing strip at the desired destination. The glide slope (or inverse of the glide ratio L/D) becomes steeper with drag, which increases with airspeed, and directly influences how much altitude is lost during travel between thermals. Therefore, sailplanes with low drag and high glide ratio across the entire flyable airspeed range (from stall to V-never exceed) clearly offer an advantage. Sailplane manufacturers therefore aggressively use the latest cutting-edge technology to increase glide ratios as far as possible within class restrictions. For example, the best glide ratio of the 15-m wingspan flapless "Standard Class" sailplane has increased from about 25 in the 1950s to 36 in the 1970s largely due to smoother laminar flow wings resulting from the use of composite materials. Computer aided wing-profile optimization, along with blended winglets and vortex generating turbulator tape or externally blown turbulators integrated with a composite wing structure have pushed the best Standard Class glide ratio to about 48 in the best

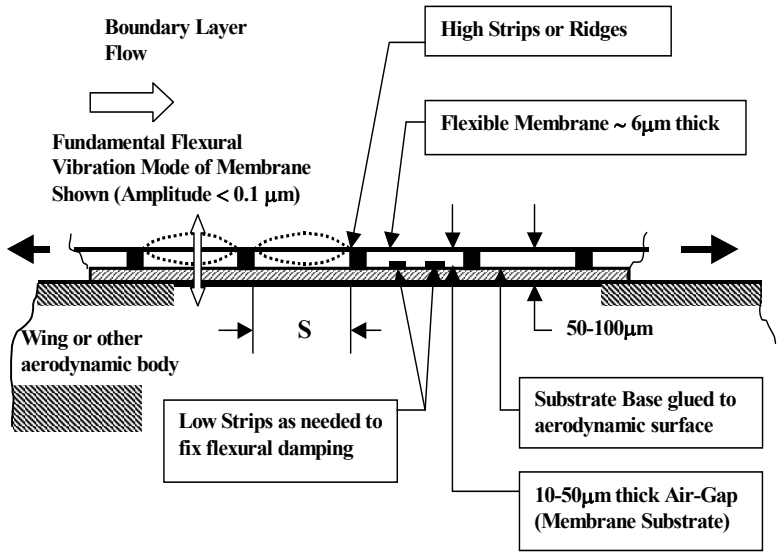

Fig 1. Schematic of the SINHA Flexible Composite Surface (FCSD)

sailplanes of the 2000-2005 generation. According to sailplane designers fundamentally new technology is needed to overcome this barrier. In this paper we present such a breakthrough based on the patent pending Sinha-FCSD[1-4].

Drag reduction and L/D increase can extend the range, endurance and speed of unmanned aerial vehicles (UAVs) and general aviation aircraft. More importantly it can lower fuel consumption and emissions of civil transport aircraft thereby directly improving the bottom line of airlines and air-cargo operators. Historically, fuel costs represented about 22% of the Direct Operating Cost (DOC) for airlines. A drag reduction of 1% can lead to a DOC decrease of about 0.2% for a large transport aircraft. Other benefits corresponding to a 1% drag reduction are 1.6 tons additional cargo or 10 additional passengers. Additionally, environmental factors, such as noise, air pollution around airports and impact on climate change, will also play an important role for future growth of the civil aviation and aircraft design. For example the main goals of vision 2020 launched by the European commission include a 50% cut in CO_2 emissions per passenger kilometer (implying a 50% reduction in fuel consumption in the new aircraft of 2020) and an 80% cut in nitrogen oxide emissions. These objectives cannot be reached without breaking through the same fundamental technological barriers that limit sailplane L/D.

A crucial barrier has been the limit on maximum possible wing drag reduction even if the currently accepted ideal of maintaining perfect laminar flow can be achieved on operational wings under "real life" conditions. The Flexible Composite Surface Deturbulator (FCSD), shown in Fig 1 can overcome this limitation by helping stabilize a slightly separated boundary layer over most of the wing chord without having it completely break away or re-attaching prematurely (Fig 3). Such a flow can not only lower skin-friction compared to attached laminar flow but can also negotiate larger adverse pressure gradients. Finally, all of this can be attained under imperfect real life conditions such as a roughened leading edge[5], which is a serious impediment to maintaining laminar flow especially on operational commercial aircraft.

In this paper we outline the concept and present recent flight-test data documenting for the first time lower sink rates and higher L/D on a test sailplane. In addition to reasons cited above, the quiescent airflow over a non powered sailplane wing provides a method for verifying wind-tunnel results at altitude at realistic flight Reynolds numbers in the absence of disturbances from propeller slipstreams and engine vibrations. Even though many serious challenges remain before the FCSD can be adapted to commercial jet transport, the drag reduction technique presented here can be upgraded for UAV use in the near term since many long-endurance UAVs are aerodynamically similar to sailplanes.

The Technology and Device

The SINHA-FCSD is a thin (under 100 μm) passive (i.e., non-powered) device (Fig 1), consisting of a flexible membrane (typically 30-300 mm wide) stretched across an array of strips on a substrate, running in the spanwise direction. The back of the substrate is bonded to the surfaces of the wing or stabilizer, typically near the aft section of the airfoil for advanced low-drag wings, where marginal separation of the attached aerodynamic boundary layer leads to large increases in drag especially for high wing loadings. Under cruising conditions, the membrane of the

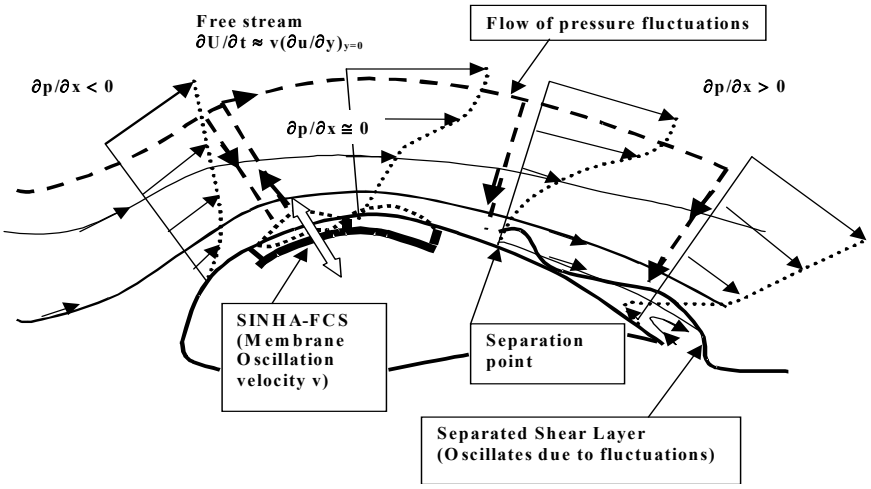

Fig 2. Schematic of the interaction of the SINHA-Flexible Composite Surface with a streamwise varying pressure gradient boundary layer on an airfoil. Thickness exaggerated

FCSD undergoes extremely small (under 0.1-μm amplitude) flow-induced flexural oscillations, which can neutralize turbulent fluctuations in the near-wall boundary layer airflow at all but a narrow frequency band. The resulting customized turbulent aerodynamic boundary layer, which is unique to the SINHA-FCSD, displays superior resistance to separation as compared to a laminar boundary layer while exhibiting lower skin-friction induced losses compared to either "naturally occurring" or artificially tripped turbulent boundary layers. This results in a reduction in wing profile drag. The current passive SINHA-FCSD concept evolved out of an earlier electrically powered Active Flexible Wall (AFW) boundary layer control concept[6] which has undergone extensive low-speed (M < 0.15) wind tunnel testing at the University of Mississippi primarily for controlling unsteady flow separation[7,8]. Unlike earlier compliant and driven flexible wall devices which were typically tested on flat-plate zero pressure gradient flow[9], the AFW and FCSD have been found to work only in boundary flows exposed to a streamwise varying pressure gradient as shown in Fig 2. To understand the flow-membrane interaction mechanism the 2-D streamwise u-momentum equation of the flow at the mean equilibrium position (y = 0) of the surface membrane of the FCSD is considered first:

$$\mathbf{v(\partial u/\partial y)_{y=0} = -(1/\rho)(\partial p/\partial x) + (\mu/\rho)(\partial^2 u/\partial y^2)_{y=0}} \qquad \mathbf{(1)}$$

The streamwise x-component of velocity "u" of the vibrating membrane (or the velocity of the fluid at the points of contact with the membrane) has been assumed to be negligible, while the wall-normal y-component of velocity "v" of the fluid next to the membrane is clearly non-zero due to membrane compliance. Key to flow-membrane interaction is the realization that the wall-normal gradient of the streamwise velocity at the wall, $(\partial u/\partial y)_{y=0}$, can be extremely large at certain x-locations. At such locations, even a small oscillation velocity (v << U) of the flexible membrane can make the $v(\partial u/\partial y)_{y=0}$ "control" term on the left hand side of equation (1) predominant enabling dissipation of turbulent kinetic energy from the freestream to the FCSD. For a non-porous, non-compliant wall, this control term is identically zero. Additionally, if the boundary layer velocity profile at the aforementioned locations is such that prior to interaction $\partial^2 u/\partial y^2_{y=0} \approx 0$, while $|(\partial u/\partial y)_{y=0}| > 0$, (i.e., u(y) is approximately linear near the wall) an order of magnitude balance of the terms in equation (1) yields:

$$\mathbf{v(\partial u/\partial y)_{y=0} \approx -(1/\rho)(\partial p/\partial x)} \qquad \mathbf{(1\text{-}a)}$$

Such a condition can be satisfied in boundary layers over curved surfaces, in the vicinity of x-locations where the streamwise pressure gradient $\partial p/\partial x$ changes from favorable ($\partial p/\partial x < 0$) to adverse ($\partial p/\partial x > 0$), as shown in Fig 2. The FCSD also passes oscillations with minimum damping at the control frequency:

$$\mathbf{f = U/s} \qquad \mathbf{(1\text{-}b)}$$

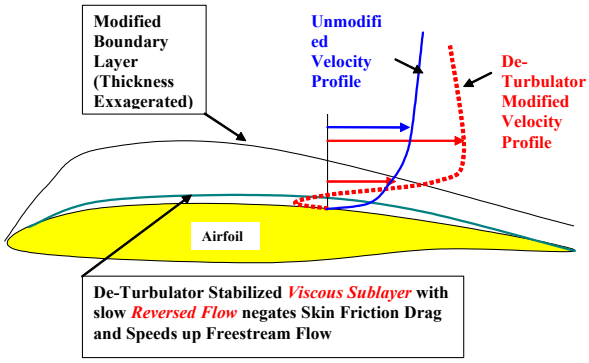

Fig 3. Depiction of Reversed Flow in Viscous Sublayer needed for Drag Reduction. Adverse Pressure Gradients cause Reversed Flow. The FCSD Attenuates Mixing across the Sublayer and keeps it from Breaking Down. (Also see Fig 27).

The aforementioned process results in sustaining fluctuations corresponding to f, while attenuating fluctuations at higher frequencies responsible for rapid mixing in regions of high shear[10]. The frequency f can be seen to correspond to a traveling-wave-flutter mode of the FCSD membrane[11]. If an adverse pressure gradient is imposed by the external inviscid flow at the downstream end (Fig 2) resulting in incipient separation, the separated shear layer is therefore prevented from thickening rapidly as a result of de-turbulation. Thus, both skin-friction and form drag are lowered. The skin-friction can be zero or negative over extended lengths, which is not doable through flow laminarization. The FCSD does not need to be directly under the shear layer since fluctuations can be propagated along the shear layer. A narrow strip of FCSD at the strategic location as per equations (1) and (1-a) is all that is needed and such a strip can attenuate turbulence from any source, including the freestream, roughened leading edge[5] or control-surface gaps.

The thin and nearly stagnant layer of air in the separated zone adjacent to the wall (Fig 3) creates an effective slip boundary condition that can accelerate the inviscid flow[5]. Thus, an FCSD treatment can also affect circulation and lift.

Experimental Verification

Many details of the aforementioned phenomenological explanation are extremely difficult to observe due to the sub-micron scales involved and have to be indirectly inferred from larger scale measurements which do not upset the process. Much of the reasoning, such as the control frequency f and flow flexible-wall interaction physics is based on earlier wind-tunnel tests with the AFW[7,8]. Hence, a decision was made to proceed with flight tests to establish the overall validity of the FCSD system as opposed to resolving small-scale details of the constituent process first.

Early tests of FCSD patches on a NLF-0414F (Ref 12) wing of a GT-3 all-composite trainer aircraft (manufactured by Global Aircraft, Starkville, MS) indicated 17-27% boundary layer momentum recovery on the top and bottom surfaces as measured in flight at Re ≈ 5-million (Refs 5 and 10). Subsequent tests on the same wing showed profile drag reductions in the range of 12-25% at Re ≈ 4 to 6-million as measured with trailing edge mounted drag rakes[12,13]. Low-speed wind tunnel tests at Re = 0.3-million on the NLF-0414F airfoil showed the FCSD capable of reducing profile drag and enhancing lift in spite of separated flow near the trailing edge[12,13], resulting in a 12% enhancement in section L/D. In all these tests the Mach numbers remained below 0.16.

Tests on the Standard Cirrus sailplane (manufactured in 1970 by Schemp Hirth, Germany; shown in Fig 4) were started since the airfoils used on the wing are capable of operating over a wider range of Reynolds numbers (0.2-4 million) without undergoing breakaway boundary layer separation. Also, the pressure distributions over these airfoils do not change drastically within this Re range even though laminar flow is maintained over about 30% of the top surface. Thus, low-speed wind tunnel results can be more readily extrapolated to flight conditions. Initial flight test results (Fig 6) for FCSD-patch installations on the bottom surface indicated a 17-27% reduction in drag (Fig 6) attributable to the bottom surface across the entire flyable airspeed range[5], even though the position of the laminar separation bubble and transition varies with airspeed on the untreated wing. Surface oil flow visualization indicated an absence of the bubble when treated with the FCSD[3].

The results presented here are a continuation of these tests. In particular the effects of treating an extensive portion of the wing and its effects on flight performance are described for the first time. Also described are important lower speed wind tunnel tests which have been used to guide the flight tests.

.

Fig 4. The Standard Cirrus, 15-m wingspan, single seat, all composite test sailplane

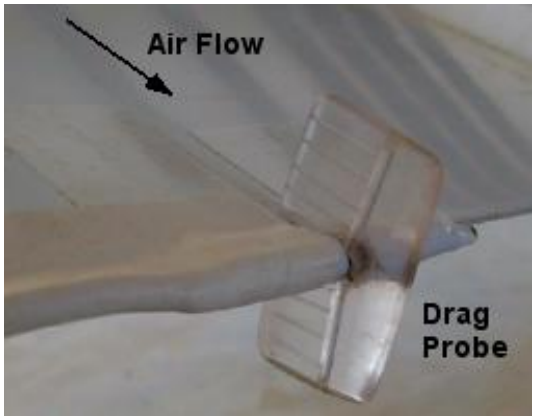

Fig 5. The drag probe mounted on the wing trailing edge. Probe has 4 equidistant stagnation ports on top and bottom 0.125" apart. Top ports are taped for wing bottom flow evaluation and vice versa

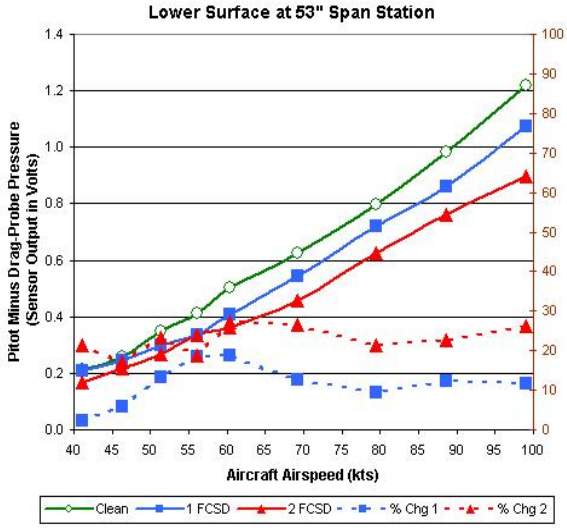

Fig.6. Drag-probe pressure sensor output (proportional to upstream stagnation pressure minus wake stagnation pressure). A reduction in output indicates drag reduction resulting from FCSD applications (1FCSD and 2FCSD) on wing bottom at the given location. % change (reduction) scale is on the right

II. Technical Approach

Sailplane Drag Reduction-Flight Tests

Initial flight tests[5] were conducted with a 600-mm long FCSD strip mounted on the lower surface of the wing of the Standard Cirrus. The strip was centered on the inboard section of the 15-m span wing, 1.32-m (52") from the wing-fuselage joint and the surface flow visualized with oil before and after the application of the FCSD shows the separation bubble on the lower surface to disappear. The 813-mm chord wing section at this spanwise location is a linear transition from the Wortmann FX S 02-196 at the root joint to the Wortmann FX 66-17 A II-182 at a spanwise location of 4.17-m outboard (beginning of ailerons). A drag probe (rake) incorporating an array of total head tubes connected to a common header (Fig 5), and encompassing 12.5-mm (1/2") of the wing top and bottom boundary layer at the trailing edge, was used to monitor changes in the wing wake. The top holes of the probe were taped off

for bottom surface measurements and vice versa. A calibrated temperature compensated differential electronic pressure transducer was used to measure the difference between the stagnation pressure from the aircraft's pitot-static probe and the integrated drag-probe stagnation pressure. The pressure transducer output (Volts) gives a direct indication of the profile drag from the wing bottom or top. A reduction in Voltage output indicated drag reduction (Fig 6).

Initial tests on the upper surface at the 52-53 inch span station did not result in drag reduction. This prompted the wind tunnel studies described below.

Wind Tunnel Setup

The SINHATECH low-speed Wind Tunnel (Fig 7) was used in these tests. The tunnel has an entrance 4-ft high and 3-ft wide with an exponential contraction down to the 12-inch high, 9-inch wide test section. Fig 8 shows a close-up of the test section showing a 5-inch chord airfoil model. For the present work a 127-mm chord, 190-mm span stereolithographed hand-smoothened and painted model of the 53-inch (1.346 m) span Standard Cirrus wing section was supported between 254-mm diameter Plexiglas disks in the test section. The disks reduce the encroachment of the airfoil-wall corner vortices towards the central section. All measurements were made on the vertical central plane. For the angles of attack investigated, the flow was found to be almost two-dimensional over 75% of the span of the test airfoil. Even though the tunnel did not employ screens or flow straighteners, the turbulence level (ratio of U-rms to U-mean) remained within 0.8% in the test section. Also, the approach velocity remained constant across the cross section of the test section, except when encountering the tunnel wall boundary layers about 0.75-inch from the walls.

FCSD Tape and Installation:

Test FCSD tapes for the wind-tunnel and flight tests were fabricated by SINHATECH using in-house prototyping facilities. The ridges (Fig 1) were 2-mm apart with a single row of low strips 15-μm lower in between the high strips. A 6-μm thick aluminized Mylar sheet, whose edges were either taped to the airfoil surface, or in the final design glued to the edges of the substrate, was used as the flexible membrane. The overall thickness of the FCSD was about 80-μm. The substrates had pressure sensitive adhesive backing and had widths varying from about 6-mm to 50-mm and lengths from 150-mm to 500-mm depending on application . The FCSD strips were oriented with the ridges on the substrate running spanwise.

Fig.7. SINHATECH Low-Speed Wind Tunnel

Data Reduction and Analysis:

The tests conducted in the wind tunnel included: (1) Total Section Drag Measurements, (2) Surface Pressure Distribution Measurements and (3) Skin Friction (Cf) Estimates

(1) ***Total Section Drag Measurements***: The total drag on the central plane was estimated by using a wake rake spanning one-chord length (5-inches or 127-mm) incorporating an array of (1/32-inch ID) total-head tubes connected to a 3/16-inch ID plenum. The rake was placed about ½-chord behind the trailing edge of the airfoil model. The difference between the upstream stagnation pressure and the pressure in the wake-rake plenum ($=\Delta P_{DR}$) indicated the loss in stagnation pressure. This indicated the total profile drag (form drag + skin friction) on the 2-D wing section. Even though, the rake was placed significantly upstream of the point where the static pressure returns to its free-stream value, the section drag coefficient c_d can be found from the following relationship[12]:

$$\mathbf{c_d = K.\ C_{pDR}.\ Y/c} \qquad \mathbf{(2)}$$

where, $C_{pDR} = \Delta P_{DR}/(\rho U_\infty^2/2)$

Y = height of the drag rake

c = the airfoil chord length

K = a constant of proportionality which can be deduced from other estimates of c_d.

U_∞ = freestream velocity = average upstream velocity in the tunnel.

ρ = freestream air density.

Since the raw pressure transducer voltage output is proportional to ΔP_{DR} for a calibrated transducer and a lower value of ΔP_{DR} implies lower profile drag, the percent reduction in the raw voltage resulting from an FCSD treatment was used to gauge its effectiveness. The same procedure was used in flight test evaluations of the FCSD.

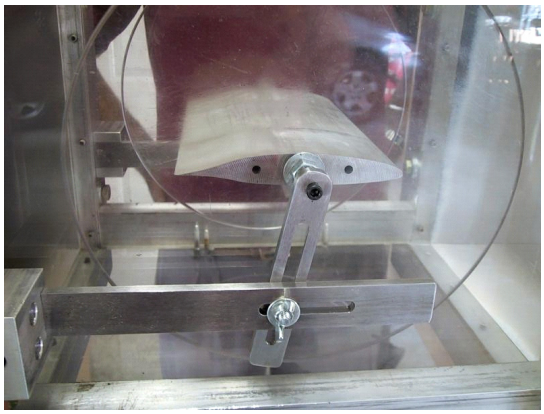

Fig 8. Close up of tunnel test section with an airfoil between end plates

(2) ***Surface Pressure Distribution Measurements*:** In order to avoid contamination of the boundary layer flow from surface imperfections the airfoil models did not have pressure taps. Surface pressure distributions were deduced from hot-wire velocity measurements of the boundary layer. A miniature single wire probe with a 5μm diameter sensor was used with a Dantec MiniCTA anemometer. The probe was calibrated in-situ in the wind-tunnel before each set of measurements. The sensor was traversed vertically through the inviscid outer part of the boundary layer at each x/c (x = position along the chord from the leading edge). The maximum time-averaged velocity during each traverse yielded the local freestream velocity U. The difference between the local static pressure p and the upstream static pressure p_∞ can be related to (U/U_∞) in terms of the local coefficient of pressure C_p as follows:

$$\mathbf{C_p = (p - p_\infty)/(\rho U_\infty^2/2) = 1 - (U/U_\infty)^2} \quad \mathbf{(3)}$$

The section coefficient of lift c_L and the section pressure-drag coefficient c_{dP} can be found from the following integrals around the contour of the airfoil:

$$\mathbf{c_L = \int C_p.d(x/c) \text{ and } c_{dP} = \int C_p.d(y/c)} \quad \mathbf{(4)}$$

Where, x/c and y/c denote the horizontal and vertical co-ordinates normalized with respect to the airfoil chord length c. Numerical approximations were used for evaluating these integrals.

(3) ***Skin Friction Estimates:*** The same hot wire sensor used for measuring the boundary layer velocity profiles The measured mean velocity profiles were integrated numerically with respect to y to obtain the displacement thickness δ_1, the momentum thickness δ_2 and the kinematic shape factor $H = \delta_1/\delta_2$. Furthermore, the momentum integral equation of the boundary layer[14] can be rewritten as follows:

$$\mathbf{C_f = \tau_w/(\rho U_\infty^2/2) = -\{(\delta_1 + \delta_2)/c\}.\{dC_p/d(x/c)\} + (1 - C_p).\{d(\delta_2/c)/d(x/c)\}} \quad \mathbf{(5)}$$

Where, τ_w = the local wall shear stress

Estimating the spatial derivatives of C_p and δ_2/c through finite difference approximations of the experimental values provided a method for estimating the local skin-friction coefficient C_f.

III. Results

Wind tunnel tests on the 5-inch (127 mm) chord Standard Cirrus 53-inch span-section airfoil model were conducted at Re = 0.3 million and M = 0.1 with and without FCSD strips. Surface oil flow patterns of the clean wing at an angle of attack $\alpha = -1°$ indicated a separation bubble on both top and bottom surfaces as the region where the oil accumulated. Even though the surface of the model had been slightly over-sanded, the positions of the separation bubble matched closely with those indicated in the surface pressure distribution plot in an XFOIL[15] simulation for this airfoil under identical conditions shown in Fig 9. The separation bubbles are seen as bulges in the C_p versus x/c

plot of Fig 9. A variety of suction side FCSD treatments were screened for this airfoil model using the drag-rake measurements for α values ranging from –2° to +2° in steps of 1°. In all FCSD cases a nominal 6-mm (0.25-inch) wide substrate was employed with the Mylar membrane taped to the airfoil surface with 32±1 μm thick Tesa tape (normally used for taping over wing-fuselage joints in sailplanes). The exact location of the FCSD strip is proprietary. The location was based on applying the criterion of Equation (1a) as far as possible with adjustment for flow features unique to this situation. The same x/c location was used for the flight tests as well.

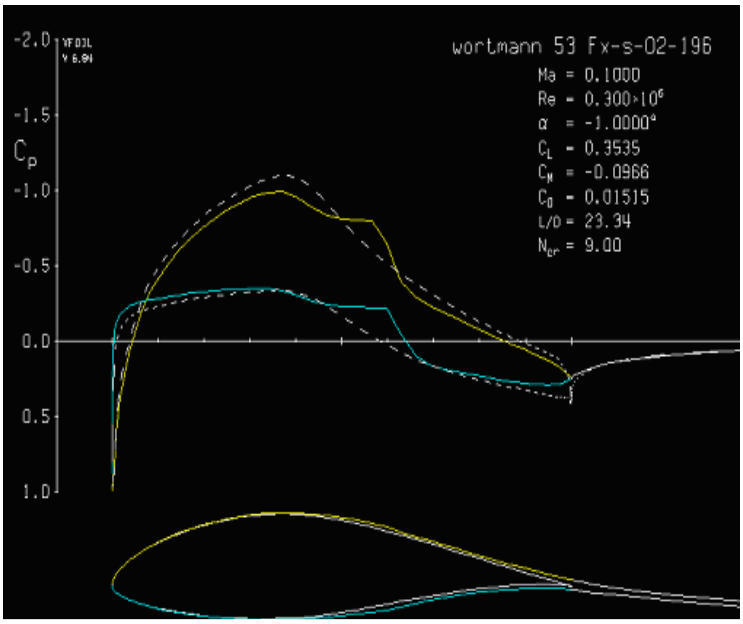

Fig.9. XFOIL Simulation of Flow on 5-inch Chord Wind Tunnel Model of Std. Cirrus 53-inch Span Airfoil Section showing C_p Distribution on Suction (yellow) and Pressure (blue) Surfaces at α = –1°, Re = 0.3 million and M = 0.1

Figs 10 and 11 show selected suction-side (i.e., top surface) boundary layer velocity profiles. The reduction in turbulence levels throughout the flow clearly demonstrates the de-turbulation effect of the FCSD. Figs 12 – 14 show the plots of skin-friction (C_f), momentum thickness (δ_2) and kinematic shape factor (H). ***The skin friction plot also shows that the FCSD reduces C_f at most locations aft of 40%-chord, demonstrating the basic drag reduction mechanism***. The momentum thickness plot indicates that the FCSD treated flow is more separated for x/c between 40 to 60%, but reattaches emphatically near the trailing edge (90%). ***The behavior of the Shape Factor H indicates the FCSD makes the boundary layer fuller (i.e. similar to turbulent BL as compared to laminar BL) anywhere the skin-friction is lowered, even though the actual turbulence levels are also lowered.***

Initial Flight-Test Validation of Drag-Reduction

In order to test the validity of the basic drag reduction mechanism elucidated in the aforementioned wind tunnel measurements, a similar FCSD installation was attempted on the 53-inch span station on the upper surface of right-hand wing of the Standard Cirrus. For the first time a reduction in drag was seen on the upper surface (Fig 15). However, Fig 15 also shows an unacceptable increase in drag at higher speeds.

The basis for drag reduction using the FCSD is to reduce skin friction by encouraging a thin and long separation-bubble like structure (Fig 3). The de-turbulation effect of the FCSD delays the rapid breakdown of the shear layer separating the bubble from the main flow. The FCSD attenuates the rapid buildup of turbulence typically found in the downstream end of laminar separation bubbles. This negates the large positive C_f values on the downstream or pressure-recovery end of the boundary layer. The adverse pressure gradient holds the near-stagnant wall-layer within the bubble against the streamwise force exerted through the shear-layer by the main flow. Since the aforementioned flows are subsonic, any reduction in downstream C_f accelerates the entire flow. This results in an increase in C_f for x/c positions upstream of the minimum pressure point. The increased upstream skin friction negates the benefit of reduction of C_f downstream, especially at higher speeds. Therefore, methods for reducing the upstream skin-friction were investigated. The solution was a backward facing step[3,4] immediately downstream of the leading edge to promote a near stagnant region between the main flow and the airfoil surface even under a favorable pressure gradient. Tests on this "Modified FCSD" installation are described below.

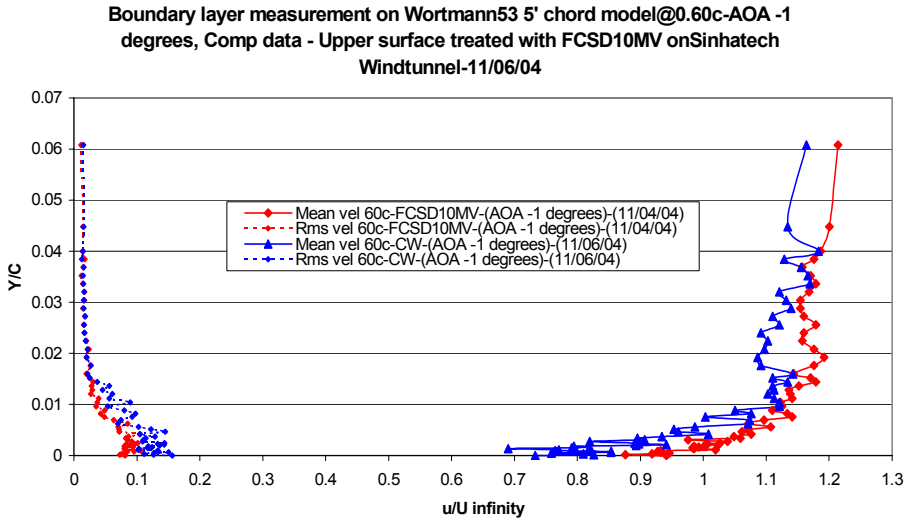

Fig.10. Suction Side Boundary Layer Velocity Profiles at x/c = 0.60 on Standard Cirrus 53-inch span airfoil model for α = –1°, Re = 0.3 M and M = 0.1 Blue-Clean Wing, Red-FCSD.

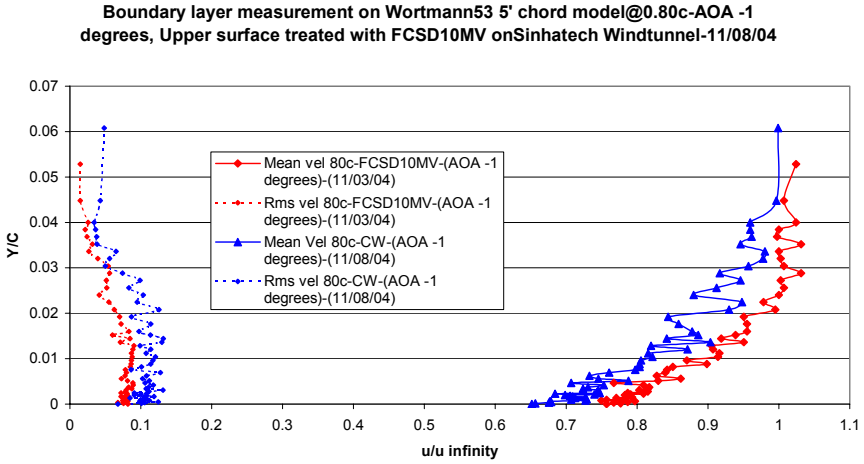

Fig.11. Suction Side Boundary Layer Velocity Profiles at x/c = 0.80 on Standard Cirrus 53-inch span airfoil model for α = –1°, Re = 0.3 M and M = 0.1 Blue-Clean Wing, Red-FCSD.

Tests with Modified FCSD

An FCSD installation on the suction-side based on the aforementioned theory indicated a slight thrust (i.e., more than 100% drag reduction!) compared to the clean airfoil in drag-rake tests in the wind-tunnel. Since the results were very repeatable, it was concluded that the treatment was extremely effective, and tunnel wall interference and blockage were responsible for over-predicting the drag reduction. Fig 16 shows the pressure distributions with and without the suction-side-only treatment for $\alpha = -1°$. ***Integration of these C_p profiles indicates an increase in section lift coefficient c_L from 0.25 to 0.62, or 148%.*** At the same time the section pressure drag coefficient c_{dP} is seen to increase from 0.02 to 0.034. However, the section L/D ratio based on the pressure drag still increased from 12 to 18.5 or 54%. The best data obtained on the wind tunnel model corresponded to a configuration of the FCSD and leading-edge step, the locations of which are proprietary.

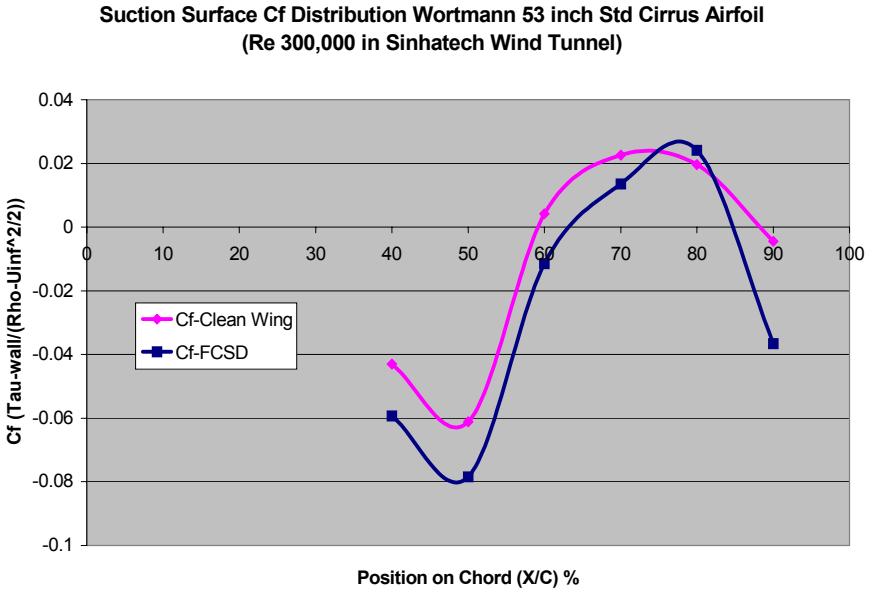

Fig.12. Measured C_f distribution on Wortmann Airfoil Model, deduced from Boundary Layer Velocity Measurements of Figs 10 and 11.

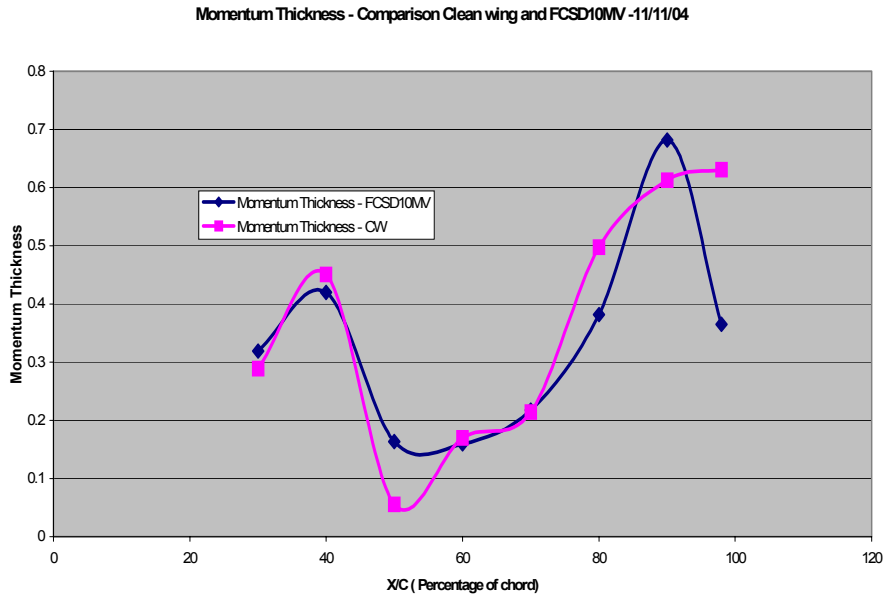

Fig.13. Momentum Thickness δ_2 distribution on Wortmann Airfoil Model, deduced from Boundary Layer Velocity Measurements of Figs 10 and 11.

In order to examine the validity of the aforementioned wind-tunnel results, an uncertainty propagation analysis was done. This yielded uncertainties of 12% in the values of $c_{L,}$ which translates to a 20% uncertainty in the 148% percent increase in c_L. Even though the experimental C_p data on the wind tunnel airfoil is close to the numerical XFOIL simulation (Fig 9), the measured c_L of 0.25 is lower than the predicted value of 0.35 primarily due to a downward due to a downward shift of the lower surface pressure data. Measurement of the lower-

surface data involved setting up the airfoil in an inverted position in the test section of the tunnel. Thus this "bias" error in the lower surface pressures was probably due to an error in α, which was accurate to only within $\pm 0.2°$. Also, the drag rake measurement at $\alpha = -1°$ showed an overall section c_d of 0.007 using K = 1 in Eqn (2), while the predicted c_d is 0.015. To reconcile the measured and predicted values, the value of K can be increased to about 2. Alternately, a bias term of 0.008 can be added to the measured c_d value. The second correction is probably more justified since it now brings the c_d of the treated airfoil model down to about 0.007. If this approach is accepted, along with the measured values of c_L the overall L/D of the test airfoil increases from 17 to 89 or 423%.

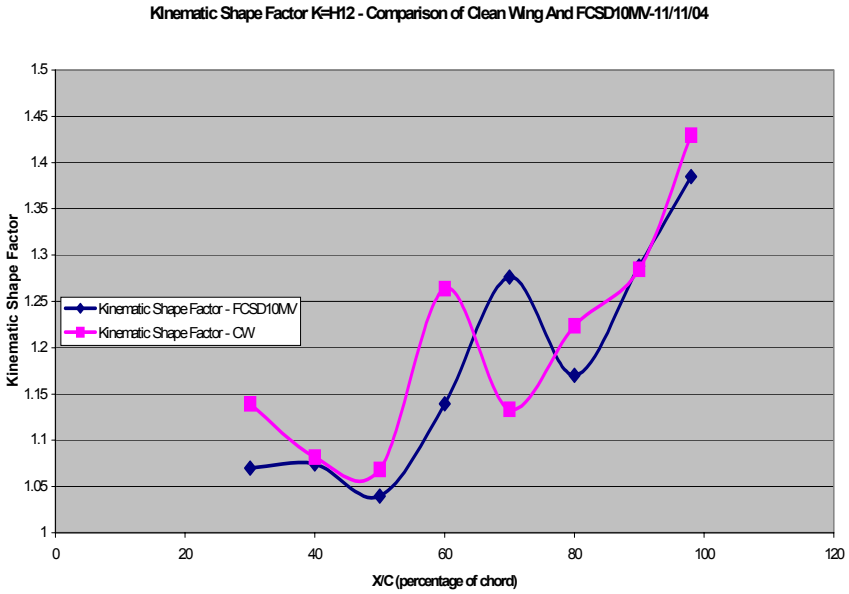

Fig.14.kinematic Shape Factor H= δ_1 /δ_2 distribution on Wortmann Airfoil Model, deduced from Boundary Layer Velocity Measurements of Figs 10 and 11.

The FCSD and leading-edge step from the wind-tunnel results were transferred to the 53-inch and 167-inch span stations on the prototype wing. Drag reductions at these two stations were observed across the airspeed range as shown in Figs 17 and 18. Apart from the drag rake data, the flight tests also provided the pilot's feedback regarding changes in handling and performance of the aircraft. Even though only two ~0.5-m long sections of the span of the right wing were treated a significant repeatable change in trim of the 15-m span sailplane was observed. Starting with take-off, the aircraft demonstrated a persistent tendency to roll to the left. This had to be corrected with opposite aileron and the corrections needed increased with speed. Also, the left wing stalled before and dropped before the right wing. These indicated that the L/D of the treated wing sections were definitely higher at all airspeeds. These were explored further through sink rate measurements described below.

IV. Sailplane Sink Rate Measurements

Additional strips of the modified FCSD were affixed so as to treat extended regions of the upper surface. The treatment was extended from the root outwards in small steps so as not to jeopardize flight safety. Significant improvements were observed when the inner 60% of the upper surface was treated while the outer sections remained untreated. With this treatment, the sailplane was found to fly in a more nose-down attitude, indicating an increase in the overall lift coefficient of the wing. The sailplane's GPS data logger was used to document altitude loss while the sailplane was flown at a specified constant airspeed in calm air above thermal activity. The rate of sink deduced from this data was used to compute the L/D glide-ratio (= Lift/Drag = Airspeed/Sink-rate) across the airspeed range. Since vertical movements of the air mass can seriously bias such measurements, at least three flights need to be

averaged (as per communications with Richard Johnson, world renowned sailplane performance tester) to obtain any meaningful drag polar (L/D versus airspeed) for comparison purposes.

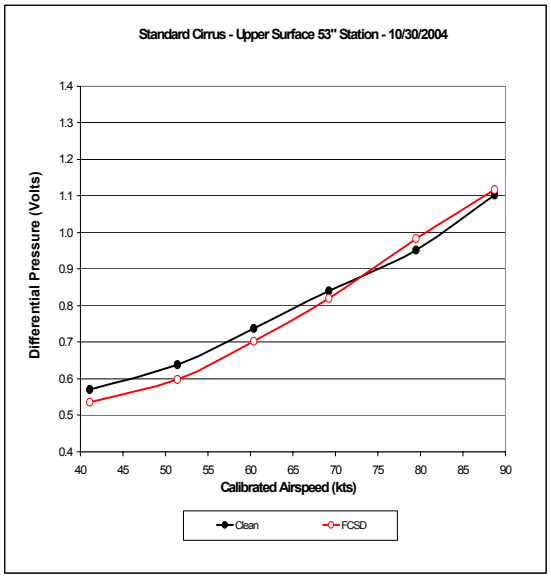

Fig 15. Drag Rake Data on First Successful Top Surface FCSD Installation at the 53-inch Span Station of the Std, Cirrus. Drag increase is seen at higher airspeeds

Fig 19 shows the averaged measured sink rates for the 60% upper surface modified-FCSD-treatment versus the untreated Standard Cirrus. Fig 20 shows the L/D versus airspeed polar. Figs 19 and 20 indicate a 5-10% reduction in sink-rates and improvement in L/D throughout the range from 40-kts (22 m/s) to about 90-kts (49.5 m/s). The maximum L/D (used to characterize sailplanes based on performance) is seen to increase from 36.0 (at about 24 m/s) to 38.7 at about 26 m/s, a 7% increase. Since these improvements are for the entire sailplane and include other sources of drag (e.g., fuselage and stabilizers), it is clear that the total wing drag reduced more than the amounts indicated by the upper-surface trailing-edge drag-rake data at the 53 and 167 inch span stations. The stall speed of the sailplane remained unchanged at about 35.5 kts (19.5 m/s), but the stall became gentler since the lift load from the outboard 40% of the wing was reduced as evidenced from a reduced bending of the wing.

Induced and Parasitic Drag

The total aircraft drag C_d equals the sum of the induced drag C_{di} (= $C_L^2/(e.\pi.A_r)$) and the parasitic drag C_{do} (also known as drag at zero lift). Since the wing lift coefficient C_L reduces with increasing airspeed, a plot of C_d versus C_L^2 over a range of airspeeds can be expected to be linear, with the slope of the line equal to $1/(e.\pi.A_r)$. Hence a least

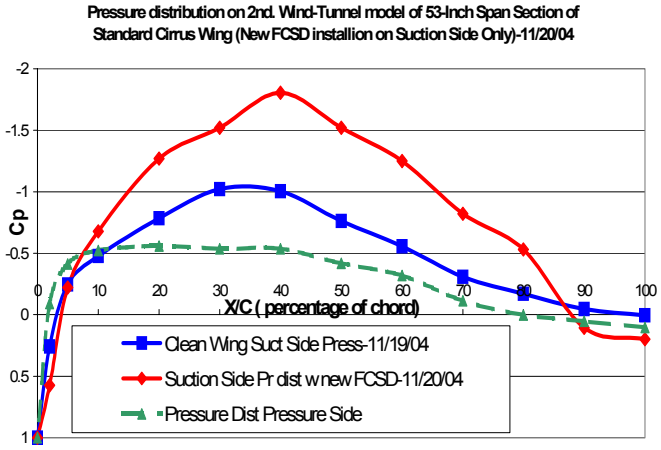

Fig.16. Measured C_p distribution on 5-inch Chord 2nd model of 53-Inch Span Section of Std Cirrus Wing Showing Effect of Modified FCSD on Suction Side. (Re = 0.3M, Ma= 0.1, α = -1°)

squares straight line fit of the C_d (deduced from measured average sink rates) and C_L^2 (measured from the airspeed and wing-loading (=weight/wing planform area)), was used to estimate C_{di}. The aforementioned 60% FCSD treatment is seen to reduce the induced drag (Fig 21), validating the lift increase in the treated sections of the wing. A decrease in parasitic drag (calculated by subtracting the induced drag from the total drag of Fig 23) is also seen in Fig 22. This is a result of reduction in wing profile drag.

Parallel Flying Tests

The FCSD strips, along with the leading-edge tapes were extended all the way to the wing tip on the top surface of the Standard Cirrus wing. This resulted in larger reduction in sink rate around 40-kts (22 m/s), with similar improvements between 60-100-kts (33-55 m/s). Fig 24 shows the output from the GPS data recorder of the treated Standard Cirrus against the same from a 2003 model higher performance ASW-28 sailplane of the same "Standard" 15-m (50 ft) wingspan class with approximately the same gross weight and wing loading (~ 7 lb_f/ft^2 = 0.3 kPa). The two sailplanes were parallel flown within about 2-wingspans at an 80-kt (44 m/s) constant airspeed based on the Standard Cirrus's airspeed indicator. This type of testing is popular among European sailplane manufacturers since the relative difference in sink-rates between the two sailplanes tends to zero out bias due to any vertical movement of the air mass. Sink-rates deduced from least-squares best-fit lines through the data points for each sailplane indicated a 12% reduction in the sink-rate of the Standard Cirrus due to the FCSD treatment as compared to the untreated Std. Cirrus (red dashed line in Fig 24.). The ASW-28 manufacturer-published (Alexander Schleicher Flugzeugbau, Germany) sink-rate polar was used as the baseline for the newer and near-pristine condition ASW-28. The ASW-28 claims a best glide ratio of 45:1 compared to the Standard Cirrus best L/D of 36:1 (based on published data and test results). In spite of the scatter in the data due to high atmospheric turbulence (typical for good soaring conditions with extensive thermal activity), the treated Standard Cirrus was seen to nearly equal the performance of the more streamlined ASW-28, even though the ASW-28 has computer-optimized laminar flow wings with micro-hole blowing turbulators on the lower surface to control flow separation and blended winglets for induced-drag reduction. Based on the best fit lines of Fig 24 the Standard Cirrus treated with the FCSD full span was sinking 6% faster than the ASW-28. The standard cirrus without the FCSD treatment would have an 18% faster sink rate.

Full-Span versus 60% Span Installation

In spite of the large and nearly identical reduction in sink-rates at 80-kts (44 m/s), the full span treatment proved inferior to the 60% treatment at about 50-kts (28 m/s) and generated more drag with speed beyond 90-kts (50 m/s). This behavior can be explained in light of the span loading tending to be more uniform as the FCSD treatment is extended. The Oswald span efficiency factor e, which is unity for an elliptical span load distribution, was determined to be 0.96 for the clean wing, 0.98 for the 60% treatment but 1.10 for the full-span treatment. Also, full-span treatment reduced the induced drag but increased the parasitic drag compared to the 60% treatment. This was believed to be a result of less than optimum treatment on the outboard sections since the optimized FCSD and leading-edge step locations were based on testing the inboard (53-inch) section in the wind tunnel.

Recent tests on a 127-mm chord model of the outboard Wortmann FX 66-17-A-II-182 airfoil modified the locations of the leading edge backward facing step (proprietary). Initial tests of this modified installation indicated a 20-30% maximum enhancement in L/D (Figs 25 and 26). Even if the worse of the two data sets is considered to be representative of an average of a larger number of data sets, it shows a treatment that should be acceptable to Standard Cirrus operators. The average of the two data sets, which incorporates reduction in the minimum sink rate at 40-kts from the worse data, shows no penalty at 50-kts, a 15% improvement between 60 and 100-kts returning to the baseline between 100-kts and V-never-exceed (110-kts). The best L/D is about 40 around 60-kts.

Even though the work to date has demonstrated that the FCSD treatment can increase L/D significantly over a wide range of airspeeds, incorrect installations and imperfections (Fig 27) as well as environmental conditions such as large changes in atmospheric temperature and humidity can lead to serious consistency problems in the real world (refer to www.sinhatech.com). However, these issues stem from the property of the materials (e.g., Mylar) and the way they are integrated into the FCSD. They do not negate the basic fluid dynamics described here. Neither do they negate the flow-membrane interaction physics exploited by the FCSD. On the positive side, in spite of their delicate construction the FCSD strips have been found to remain intact and workable on the wing in the face of debris and regular handling of the sailplane. The consistency problems need to be overcome before making the technology commercially available to any aircraft. Our present efforts are therefore focused on addressing this.

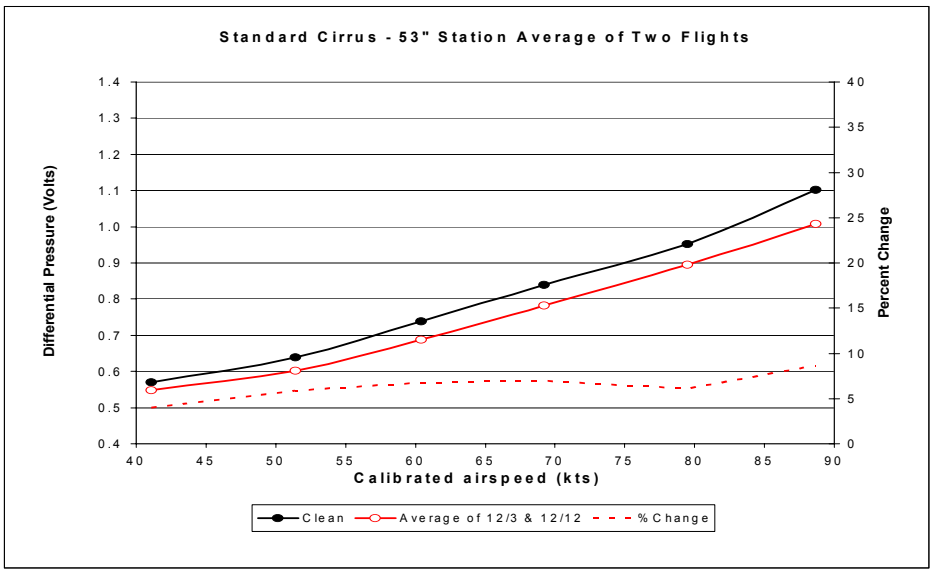

Fig.17: Drag Rake Data on Modified Top Surface FCSD Installation at the 53-inch Span Station of the Std. Cirrus. Drag Reduction increases at high airspeeds

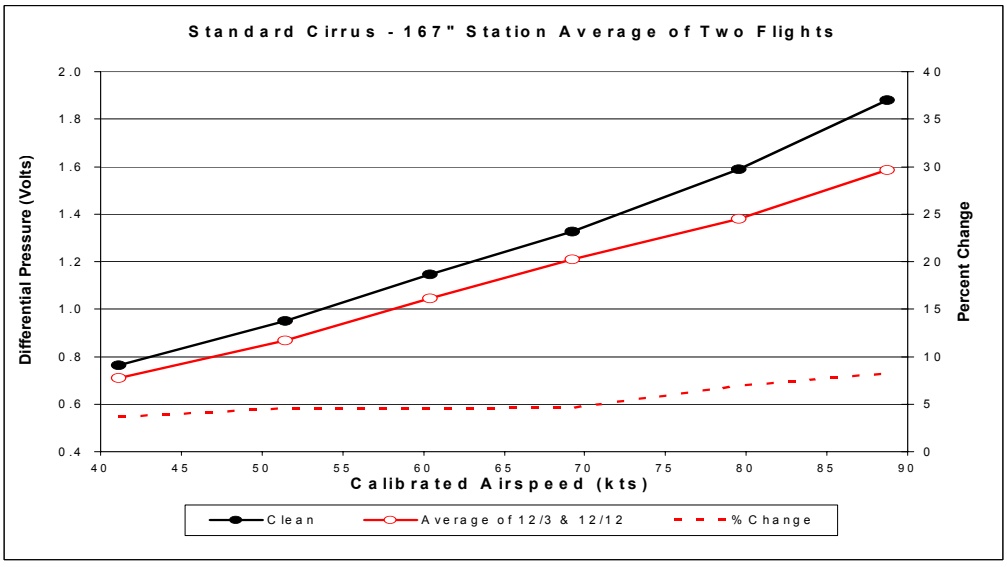

Fig 18: Drag Rake Data on Modified Top Surface FCSD Installation at the 153-inch Span Aileron Station of the Std. Cirrus. Drag Reduction increases at high airspeeds

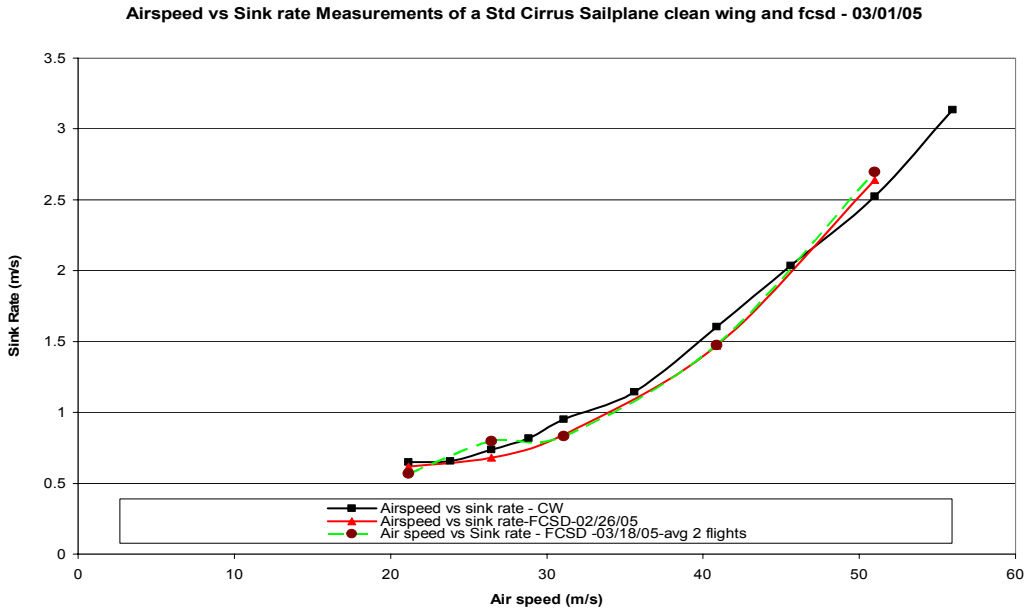

Fig 19: Sink rate measurements of a Standard Cirrus sailplane - shows the changes with a 60 % span (red) and a complete span (green) FCSD treatment.

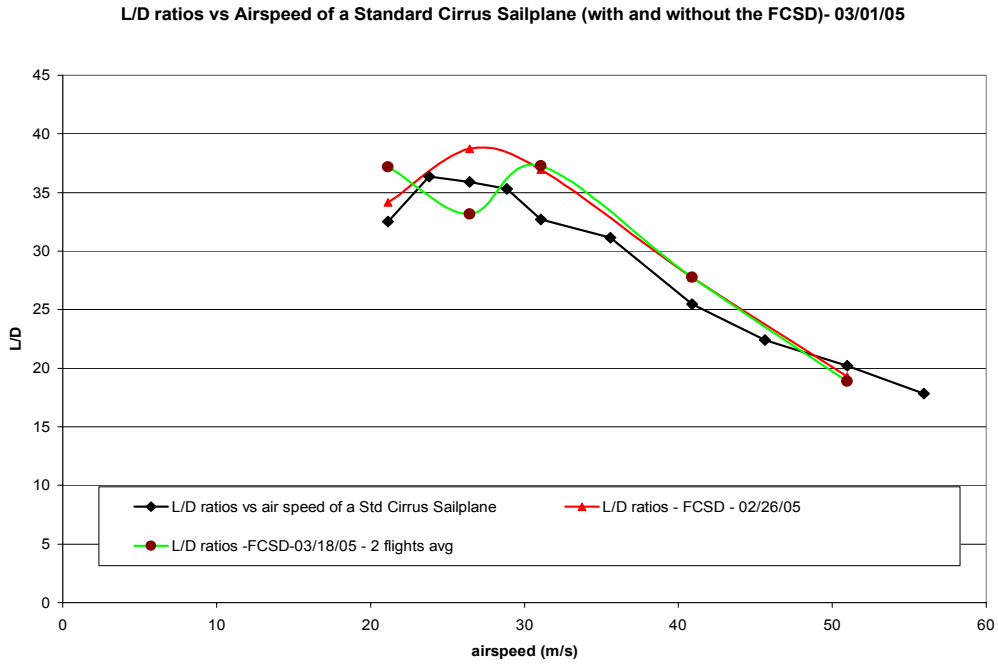

Fig 20: L/D changes of a Standard Cirrus sailplane with a 60 %(red) and a complete span (green) FCSD treatment.

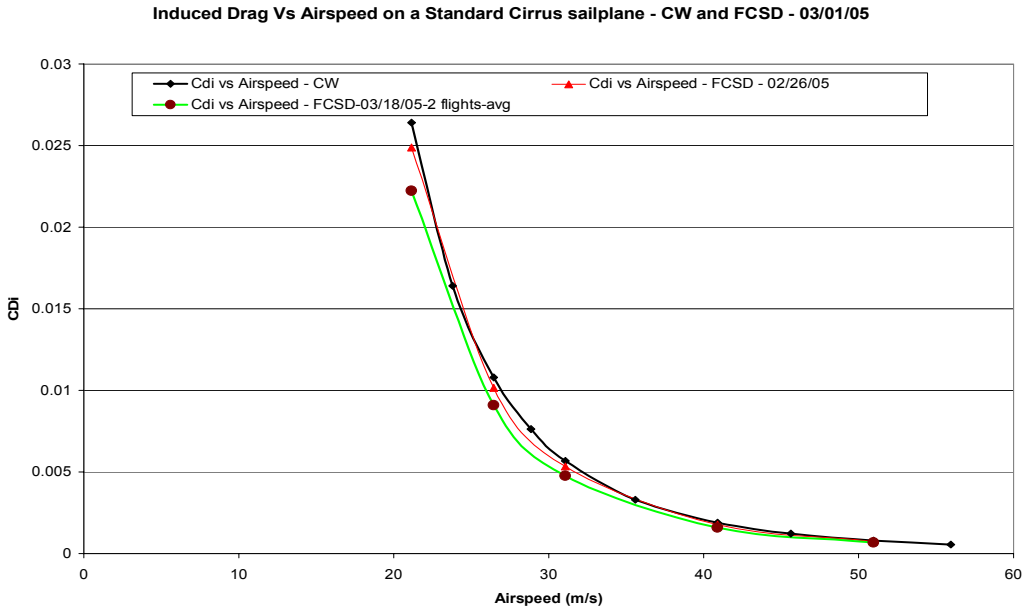

Fig 21: Induced Drag changes of a Standard Cirrus sailplane with a 60 %(red) and a complete span (green) FCSD treatment.

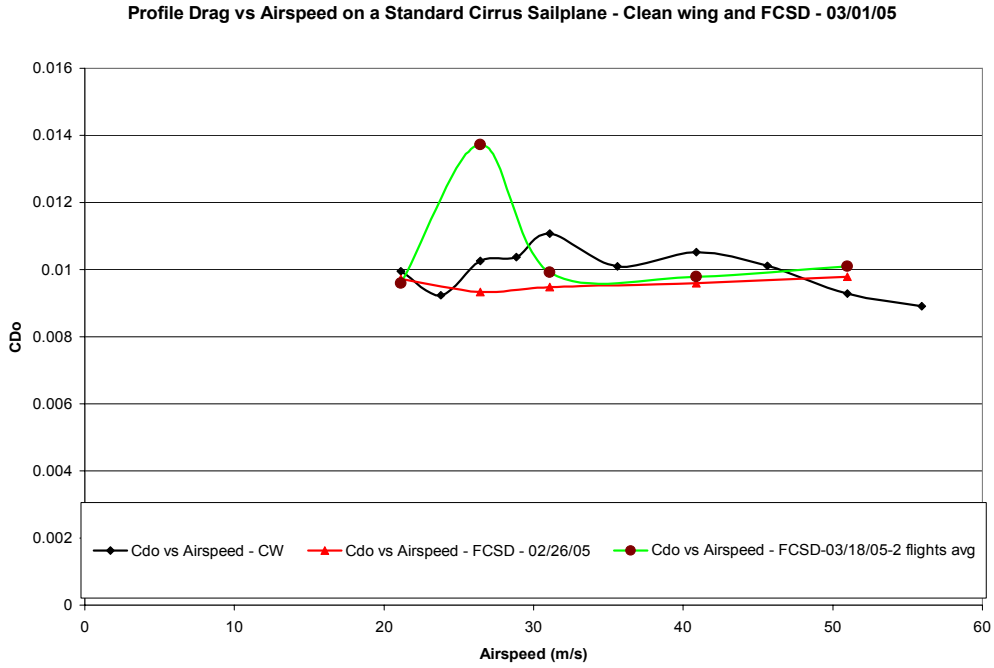

Fig 22: Parasitic Drag changes of a Standard Cirrus sailplane with a 60 % (red) and a complete span (green) FCSD treatment.

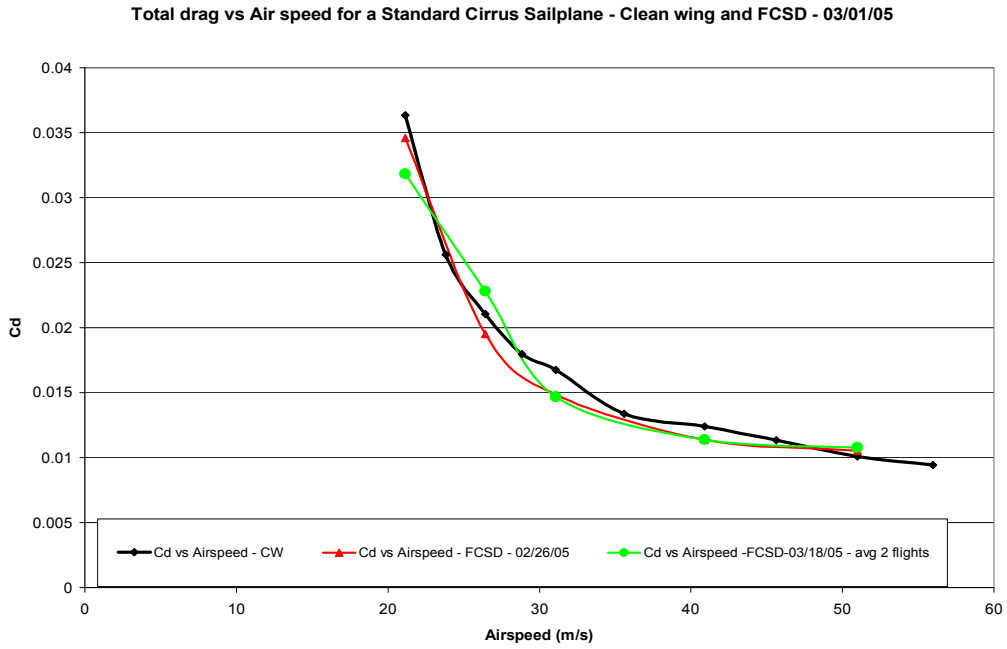

Fig 23: Total Drag changes of a Standard Cirrus sailplane with a 60 %(red) and a complete span (green) FCSD treatment.

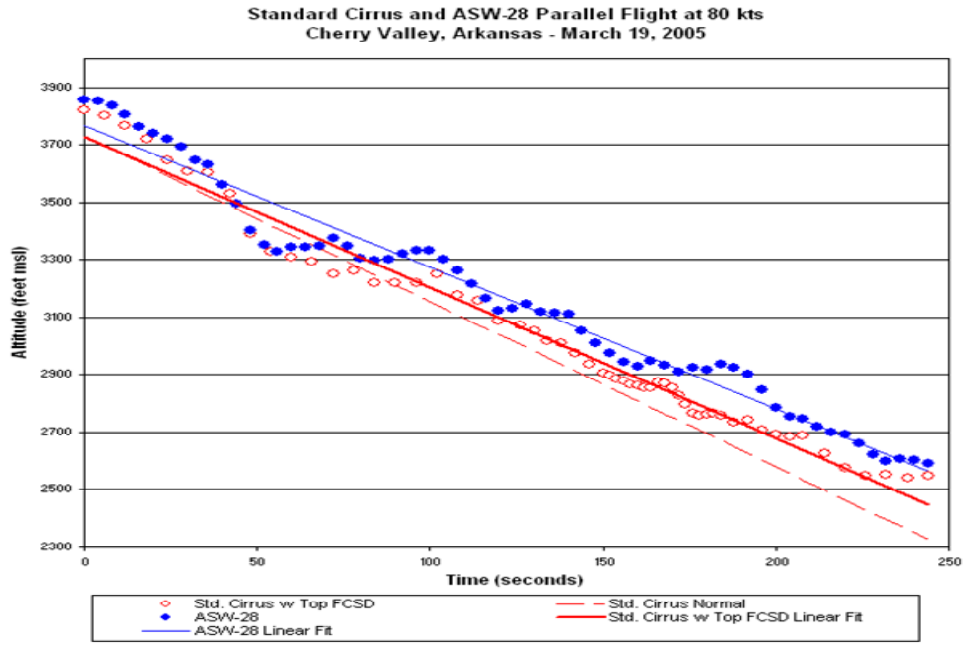

Fig 24: Parallel flight measurement with a ASW-28 sailplane. Standard cirrus sailplane has an 18% faster sink rate without the FCSD.

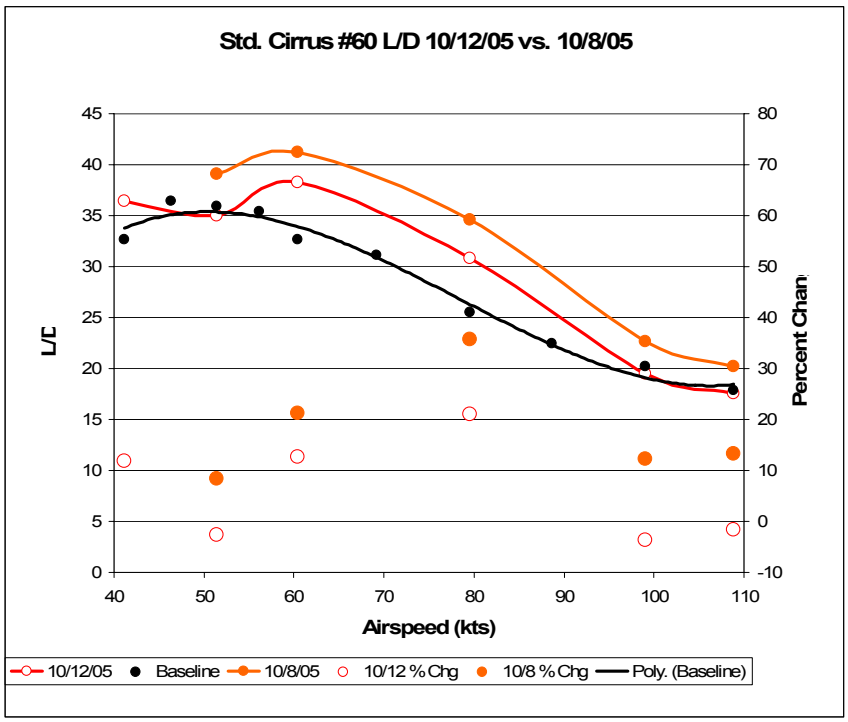

Fig 25: Standard Cirrus L/D for two flights with modified full-span FCSD treatment

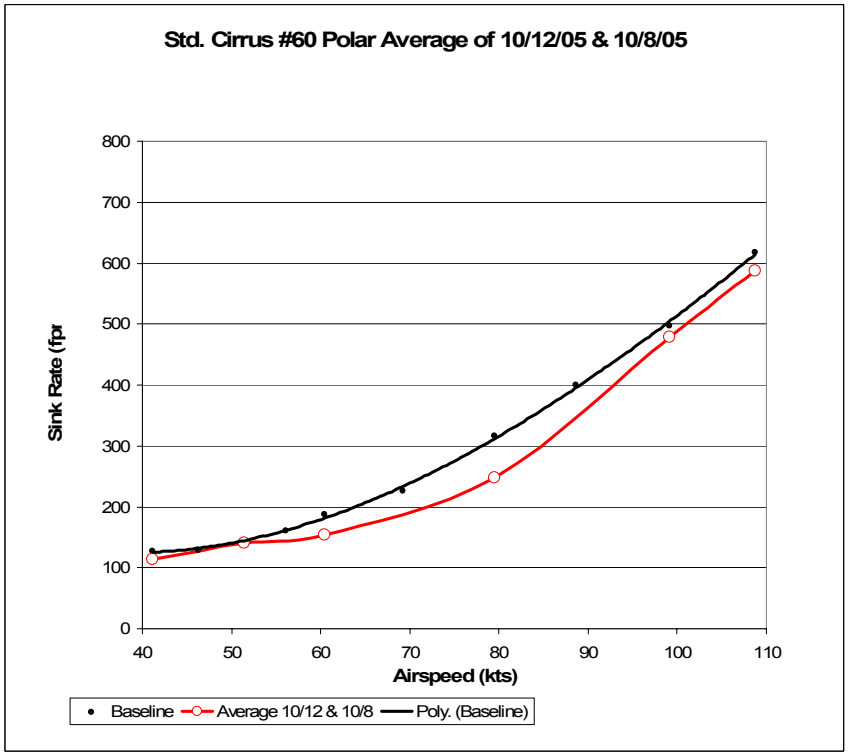

Fig 26: Standard Cirrus averaged sink rates from the two curves of Fig 25.

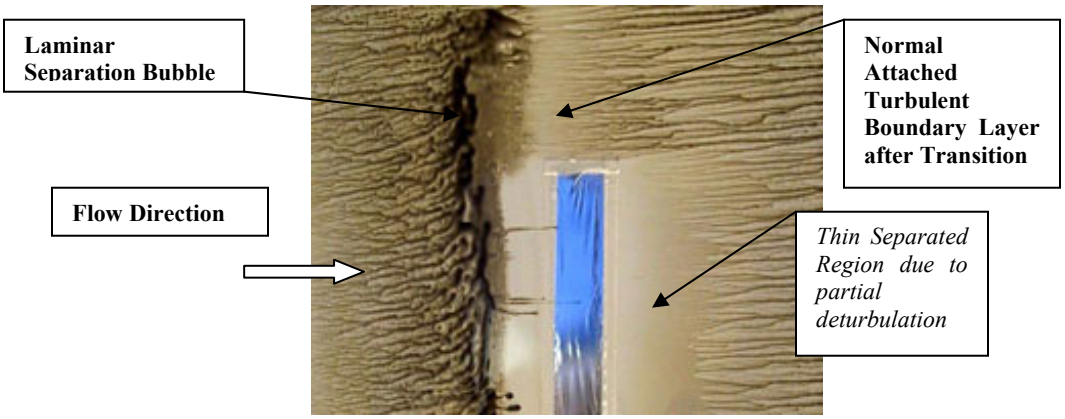

Fig 27. Surface oil flow visualization showing effect of imperfections and wrong location of FCSD on deturbulation efficacy. The flow is modified but the separation bubble is not removed.

V. Conclusions

A passive flexible wall flow control device has been developed that can be affixed to selected x/c locations on an aircraft wing surface to reduce wing profile drag as well as induced drag as evidenced from sailplane sink rate measurements. The locations are critical, and incorrect locations can increase drag.

Wind tunnel tests have shown that the FCSD promotes a thin separated flow region near the airfoil surface. This "slip layer" is estimated to be a fraction of a micron thick (Figs 3 and 27) for the flows considered and do not show up in the hot-wire measurements near the wall. It is however visible in surface oil flow visualizations and its effect shows up in skin friction (C_f) estimates from boundary layer momentum integrals. A backward facing step near the leading edge can help establish the slip layer in regions where the freestream pressure gradient is favorable. The de-turbulation effect needed for sustaining such layers is also evidenced from reduced boundary layer velocity fluctuation measurements.

When mounted on the upper surface of an airfoil, the FCSD speeds up the freestream flow, yielding lower pressures (C_p) and higher lift. The increased lift lowers the wing angle of attack and thus the induced drag. The profile drag is reduced primarily due to skin friction reduction, although reduction in turbulent dissipation may also be a factor. Because of the slip layer, the skin friction can be lower than with perfect attached laminar flow.

The spanwise distribution of the FCSD treatment can be used to modify the span loading of a wing and enhance its Oswald span efficiency.

The FCSD can readjust to widely varying flow conditions brought about by a change in airspeed. However the drag reduction and enhancement in L/D varies with airspeed. Based on the tests conducted here, a minimum L/D enhancement of 7-10% across a wide airspeed range appears possible for the 1970 era Standard Cirrus, with the maximum L/D increasing by 7-11%, depending on treatment (full or partial). However, for a more restricted range of airspeeds, the enhancement can be more than 20%. Since L/D enhancements of the wing section can be as high as 400%, as deduced from the wind tunnel tests, an aircraft with a more streamlined fuselage or a flying wing configuration can be expected to benefit more from this technology.

Finally, the repeated sink-rate reductions and L/D enhancements demonstrated here on an actual sailplane have clearly validated the feasibility of the FCSD drag reduction concept for aircraft with similar wing profiles and flow characteristics. The FCSD can therefore be seriously considered for long-endurance UAVs, as well as small low-speed general aviation aircraft with smooth wing surfaces.

Acknowledgments

The author would like to thank Oxford Aero Equipment, Oxford, MS for providing the test aircraft and conducting the flight tests. Acknowledgements are also due to the National Science Foundation (Award no. 0420115) for supporting significant parts of the research presented here.

References

[1] Roake, J.H., ed.**,** "Sailplane Performance Increases You Can Only Dream About: Meet Sumon Sinha," New Zealand Gliding Kiwi, June-July 2005, Vol.28, No. 9., pp. 12-18.

[2] Sinha, S.K., "System and Method for Using a Flexible Composite Surface for Pressure-Drop Free Heat Transfer Enhancement and Flow Drag Reduction," U.S. Patent Application fied Jan 31, 2003, PCT Intl Patent Application filed Feb 3, 2003. (USPTO Pub. No. US-2003-0145980-A1, Aug 2003).

[3] Sinha, S.K., "System and Method for Enhancing Lift and Reducing Flow Drag with a Flexible Composite Surface," U.S. Provisional Patent Application No., 60/666,639, Filed March 29, 2005.

[4] Sinha, S., and Sinha, S.K.**,** **"**A Method For Reducing Drag of Slender Objects," U.S. Provisional Patent Application, Filed March 30, 2005.

[5] Sinha, S.K., "Aircraft Drag Reduction with Flexible Composite Surface Boundary Layer Control," (AIAA 2004-2121), 2nd. AIAA Flow Control Conference, 28 Jun-July 1 2004, Portland, OR.

[6] Sinha, S.K.; "System for Efficient Control of Flow Separation using a Driven Flexible Wall," U.S. Patent No. 5,961,080, October 5,1999.

[7] Mangla, N.L., "Controlling Dynamic Stall with an Electrically Actuated Flexible Wall," Ph.D. Dissertation, Mech Eng Dept, University of Mississippi, December 2002.

[8] Sinha, S.K., "Active Flexible Walls for Efficient Aerodynamic Flow Separation Control" (AIAA Paper 99-3123), Norfolk, VA June 26-29, 1999.

[9] Bushnell, D.M. and Hefner, J.M., "Effect of Compliant Wall on Turbulent Boundary Layers," *Physics of Fluids,* Vol. 20, No. 10., Pt II, Oct 1977, pp. s31-s48.

[10] Sinha, S.K.,., "Flow Separation Control with Microflexural Wall Vibrations," *Journal of Aircraft*, Vol.38, No.3., May-June-2001, pp. 496-503.

[11] Carpenter, P.W., Lucey, A.D. and Davies, C., "Progress on the Use of Compliant Walls for Laminar Flow Control," *J. of Aircraft*, Vol.38, No.3, 2001, pp. 504-512.

[12] Sinha, S.K., 2004c., "Micro-Flexural Composite Surface for Aircraft Drag Reduction," Final Report Phase-I, NASA Contract NNL04AA32C, LaRC, Hampton, VA; July 30, 2004.

[13] Ravande**,** S.V., "Performance Improvement and Drag Reduction of Aircraft by Boundary Layer Control using a Flexible Composite Surface Deturbulator," M.S. Thesis, Mechanical Engineering Department, University of Mississippi, August 2005.

[14] Schlichting, H. , 1979, *Boundary Layer Theory*, McGraw Hill.

[15] Drela, M., 1996: XFOIL-Code for 2-D Airfoil Flow Computations, Mass Inst. Of Tech, Cambridge, MA